You might find this additional information useful...

Supplemental material for this article can be found at:
http://jn.physiology.org/cgi/content/full/00865.2005/DC1

This article cites 49 articles, 26 of which you can access free at:
http://jn.physiology.org/cgi/content/full/95/1/535#BIBL

This article has been cited by 2 other HighWire hosted articles:

Efficient Estimation of Detailed Single-Neuron Models
Q. J. M. Huys, M. B. Ahrens and L. Paninski
J Neurophysiol, August 1, 2006; 96 (2): 872-890.
[Abstract] [Full Text] [PDF]

The Interplay Between Homeostatic Synaptic Plasticity and Functional Dendritic Compartments
I. Rabinowitch and I. Segev
J Neurophysiol, July 1, 2006; 96 (1): 276-283.
[Abstract] [Full Text] [PDF]

Updated information and services including high-resolution figures, can be found at:
http://jn.physiology.org/cgi/content/full/95/1/535

Additional material and information about *Journal of Neurophysiology* can be found at:
http://www.the-aps.org/publications/jn

This information is current as of November 15, 2006 .

Fast Functional Imaging of Single Neurons Using Random-Access Multiphoton (RAMP) Microscopy

Vijay Iyer,[1,2] Tycho M. Hoogland,[1] and Peter Saggau[1]

[1]*Department of Neuroscience, Baylor College of Medicine; and* [2]*Department of Electrical and Computer Engineering, Rice University, Houston, Texas*

Iyer, Vijay, Tycho M. Hoogland, and Peter Saggau. Fast functional imaging of single neurons using random-access multiphoton (RAMP) microscopy. *J Neurophysiol* 95: 535–545, 2006. First published October 12, 2005; doi:10.1152/jn.00865.2005. The successful study of dendritic signaling and computation requires the ability to simultaneously monitor neuronal activity at multiple cellular sites. While the difficulties of accessing dendritic submicron structures with conventional micropipette approaches are generally overcome by optical recording techniques, their spatio-temporal resolution has limited such studies to few sites or slow signals. Here we present a novel approach to functional imaging, termed random-access multiphoton (RAMP) microscopy, which combines multiphoton excitation with an inertia-free scanning mechanism. RAMP microscopy employs two-dimensional acousto-optic deflection to rapidly position a focused near-infrared ultrafast laser beam between dwell periods at multiple user-selected sites. Because neuronal structures are generally sparse, activity located throughout various compartments, including thin dendritic branches and spines, can be mapped at high frame rates while maintaining the signal-to-noise ratio of conventional scanning microscopy. Moreover, RAMP microscopy maintains the excellent structural imaging capability of multiphoton excitation, i.e., intrinsic optical sectioning and high lateral resolution from within highly light-scattering brain tissue. RAMP microscopy thus comprises a versatile tool for investigating correlations of dendritic structure and function with significantly enhanced experimental throughput.

INTRODUCTION

The dendrites of central neurons are the substrate of substantial computational power (Hausser and Mel 2003). The nonuniform spatial distributions of branches, receptors, and voltage-gated channels throughout these dendrites have been related to various rules of compartmentalized cellular excitability, dendritic integration, and plasticity (Goldberg and Yuste 2005; Johnston et al. 2003; Polsky et al. 2004; Schaefer et al. 2003; Zhang and Linden 2003). Optical recording techniques based on fluorescent indicators enabled generation of the first spatiotemporal "maps" of dendritic function using conventional wide-field imaging based on CCD cameras (Jaffe et al. 1992; Regehr and Tank 1992; Tank et al. 1988) or photodiode arrays (Regehr et al. 1992; Ross and Werman 1987). These pioneering efforts provided early evidence of segregated signaling in dendrites but were limited in spatial resolution to coarsely defined dendritic regions.

Advances in optical techniques have since allowed functional maps to be obtained with increasing spatiotemporal resolution. An indirect application is the use of infrared optical microscopy, which has enabled micropipettes to physically access and electrically record from dendritic processes (Stuart et al. 1993). This technique provides unrivaled signal resolution and has yielded much insight into the distribution of channels along primary dendritic structures over the past decade (Johnston et al. 2003). However, micropipette approaches cannot be readily extended to more than a handful of recording sites (Larkum and Zhu 2002) nor to structures of dimension approximately ≤1 μm. These fine structures include the many thin oblique and basal branches of pyramidal neurons—where most excitatory synapses are located (Megias et al. 2001). In addition, the dendrites of the wide array of interneurons in the CNS are generally of small diameter (Goldberg et al. 2005).

Improved techniques for direct optical recording have, meanwhile, enabled access to these important thin dendritic structures. These techniques include modern wide-field microscopy systems employing enhanced imaging detectors—both fast cooled CCD cameras (Djurisic et al. 2004; Frick et al. 2003; Larkum et al. 2003) and high-density photodiode arrays (Antic et al. 1999). The use of imaging detectors is attractive because they allow "parallel" mapping of dendritic function, in contrast to the "serial" approach of micropipette recordings. Unfortunately, despite the considerable improvements, the spatial resolution, contrast, and depth penetration of these wide-field techniques remain limited owing to the considerable light scattering of living brain tissue. Laser scanning microscopy (LSM) approaches with optical sectioning capability, on the other hand, allow clear resolution of thin branches and even dendritic spines within brain tissue. Both confocal laser scanning microscopy (Hoogland and Saggau 2004; Jaffe et al. 1994) and multiphoton laser scanning microscopy (Yasuda et al. 2003; Yuste and Denk 1995) have been applied to optical recording from dendritic structures. However, current LSM systems do not allow for simultaneous measurement from discontiguous sites, owing to their typical reliance on inertia-limited scanning mechanisms (e.g., galvanometer-driven mirrors). This entails the use of line-scanning protocols to achieve sampling rates sufficient to record physiological signals. Because such scan lines can intersect only a very small number of sites-of-interest in complex neuronal structures, a "serial" approach of mapping dendritic excitability or activation one site at a time has been employed (Frick et al. 2003; Goldberg et al. 2005; Kaiser et al. 2001; Svoboda et al. 1999; Waters et al. 2003).

Address for reprint requests and other correspondence: Peter Saggau, Department of Neuroscience, One Baylor Plaza, S603, Houston, TX 77030, Tel: (713) 798-5082, Fax: (713) 798-3946, Email: psaggau@bcm.tmc.edu

Here we report on a new technique, termed random-access multiphoton (RAMP) microscopy. It combines the intrinsic optical sectioning advantage of multiphoton excitation (Denk et al. 1990) with the ability to record concurrently from many sites throughout the field of view. RAMP microscopy employs two orthogonal acousto-optic deflectors (AODs) that steer a pulsed infrared laser beam suited for multiphoton excitation in an inertia-free manner, enabling the femtoliter multiphoton excitation volume to be laterally repositioned arbitrarily within the microscope's specimen plane with very short latency (~15 μs for the high-resolution deflectors used here). In the study of individual neurons, the laser beam can thus exclusively visit dendritic sites of interest in rapid succession. Because neuronal structures are sparse, high sampling rates (≥ 1 kHz) can be obtained simultaneously at all sites while still dwelling sufficiently long to maintain the signal-to-noise ratio (SNR) of conventional scanning systems. RAMP microscopy thus allows high-resolution, high-speed functional imaging, enabling global or regional spatiotemporal maps of fast intracellular signals within individual neurons to be obtained within single experimental sessions.

As an initial demonstration, we employed the developed instrument to obtain readily spatial maps of back-propagating action potential (bAP) entry into thin oblique branches of hippocampal CA1 pyramidal neurons both in control conditions and in the presence of a pharmacological blocker. We envision that RAMP microscopy will enable a variety of such high-throughput mapping protocols in the dendrites of central neurons. Future applications should include multi-site stimulation of neurons using caged compounds as well as recordings from neuronal populations.

METHODS

AODs

The operation of most AODs can be described by the Bragg effect (Gottlieb et al. 1983), for which the deflection angle is given by

$$\theta = \frac{\lambda f}{v_{acoustic}} \qquad (1)$$

where λ is the optical wavelength, f is the frequency of the acoustic wave, and $v_{acoustic}$ is the velocity of the acoustic wave (Fig. 1A). Thus
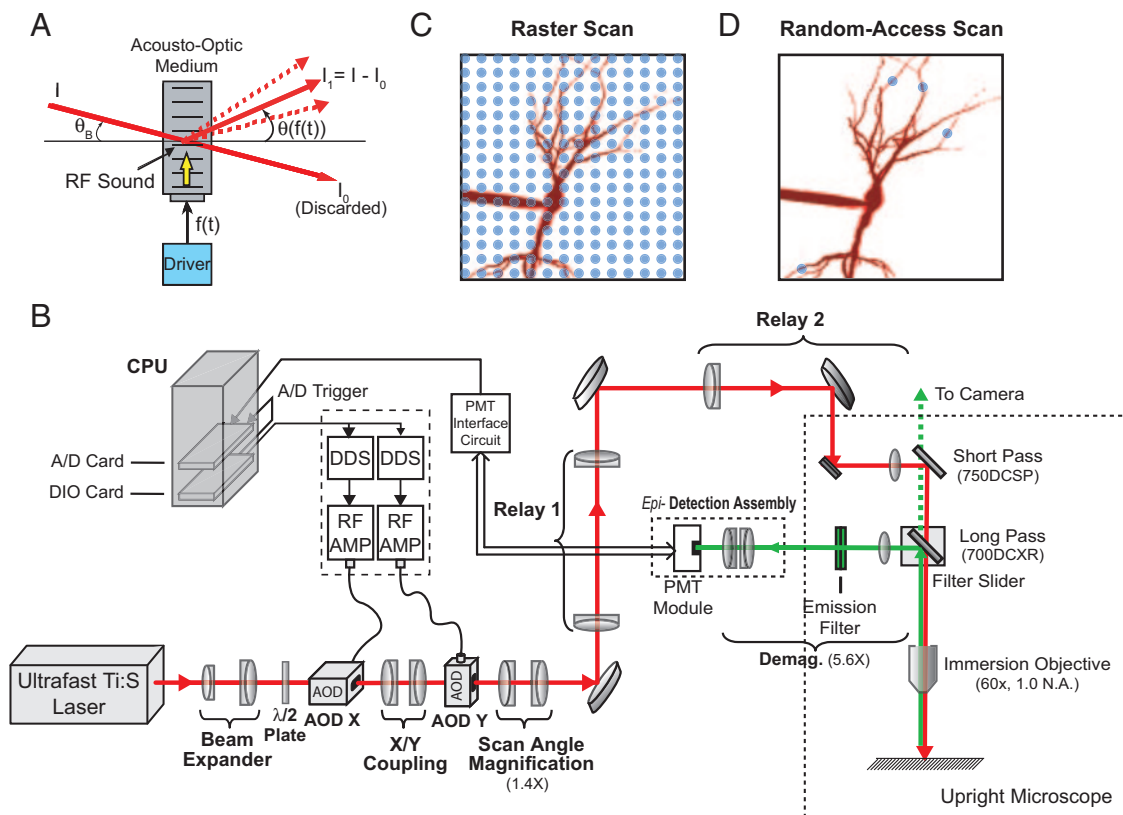

FIG. 1. Principles and design of random-access multiphoton (RAMP) microscope. *A*: scan angle $\theta[f(t)]$ of a laser beam in the 1st diffraction order of an acousto-optic deflector (AOD) is controlled by time-varying acoustic frequency $f(t)$. For a beam incident at the Bragg angle (θ_B), most of the intensity I is deflected into the 1st diffraction order I_1. *B*: RAMP microscope system overview. Output beam from a pulsed ultrafast Ti:S laser is expanded and adjusted for optimal linear polarization via a half-wave ($\lambda/2$) plate. Beam passes through 2 orthogonally mounted AODs, producing arbitrary 2-dimensional angular scan pattern. Scan pattern is controlled by the programmed frequencies of pure tone RF signals generated by direct digital synthesis (DDS), which are amplified (RF AMP) and coupled to the 2 deflectors. Optical path between and subsequent to 2 AODs consists of several relay telescopes—lens pairs separated by the sum of their focal lengths. These relay common angular pivot point plane to the back focal aperture of a ×60/1.0 NA water-immersion objective, which converts scan pattern from angular to lateral. "Scan angle magnification" telescope serves to increase scan range by 1.4× per dimension to span much of objective's field of view. Emitted fluorescence is collected via objective and demagnified onto cathode of a PMT module, the gain and output signal of which are controlled and conditioned, respectively, by a custom PMT interface circuit. Custom software for system manages digital input/output (DIO) and A/D (A/D) boards that interface to the DDS and PMT detection circuitry, respectively. Software allows operation in 2 modes—raster scanning (*C*) and random-access scans (*D*). In the former case, beam visits a high-density square array of scan sites to collect structural images. In the latter, beam visits a sparse set of user-selected scan sites for fast functional imaging at structures of interest.

the angular scan range of a deflector is determined by $\Delta f\theta = (\lambda\Delta f)/v_{\text{acoustic}}$, where Δf is the acoustic frequency bandwidth. An AOD device can be characterized by its resolution N, also referred to as its time-bandwidth product, given by (Gottlieb et al. 1983)

$$N = \frac{D\Delta f}{v_{\text{acoustic}}} = \Delta f\tau_{\text{access}} \qquad (2)$$

The value N specifies the number of resolvable angles across the angular scan range of the deflector after accounting for diffraction at the AOD aperture, assuming the beam fills the aperture as was the case here. Here, D is the optical aperture size in the dimension of beam deflection and $\tau_{\text{access}} = D/v_{\text{acoustic}}$ is the "access time"–the time required for the acoustic wave to traverse the optical aperture—which determines how fast the beam can be repositioned.

The custom AODs (ATD-7010CD2, IntraAction, Belwood, IL) employed were specified to have large square optical apertures (10 × 10 mm) to achieve high-resolution imaging and to allow a straight-forward optical design based on spherical optics. In particular, the slow-shear acoustic mode of TeO_2 was elected as it has a sufficient acousto-optic figure of merit to support high-efficiency acousto-optic interaction in such a large volume with modest device size (25 mm path length) and acoustic power (<2 W). The employed AODs were able to provide efficient (>50%) diffraction efficiency—the percent of light in the first diffraction order that scans according to *Eq. 1*—over an acoustic frequency bandwidth $\Delta f = 40$ MHz (50–90 MHz), and the slow-shear acoustic mode waves in TeO_2 travel at $v_{\text{acoustic}} = 660$ m/s. Thus employing *Eqs. 1* and *2*, the angular scan range is $\Delta\theta = 49$ mrad and the resolution $n = 606$. This resolution is sufficient to support the possibility of diffraction-limited imaging (~300 nm) within a 200 × 200 μm scan area. Such a large field of view was deemed a design criterion to allow visualization of significant portions of neuronal dendrites. Meanwhile, the access time $\tau_{\text{access}} = 15$ μs, was sufficiently short to support a maximal scan rate of 66 kHz (= $1/\tau_{\text{access}}$).

To generate the acoustic waves, each deflector is driven by tunable RF waves generated by direct digital synthesis (DDS) boards (AD9852/PCB, Analog Devices, Norwood, MA). Direct digital synthesis of the RF waves was chosen for its superior frequency stability (±0.004%) and linearity relative to traditionally used voltage controlled oscillators (VCOs). These electrical RF signals are converted into acoustic waves by a piezoelectric transducer bonded to the TeO_2 crystal.

Optical paths and adjustments

An overview of the RAMP microscope system is provided in Fig. 1*B*. A femtosecond Ti:S laser (Mira 900D, Coherent, Santa Clara, CA) was pumped by an 8 W, 532 nm diode-pumped solid-state laser (Verdi-8, Coherent). A portion of the output beam was reflected into a laser spectrum analyzer (not shown, E201LSA03, Imaging and Sensing Technologies, Horseheads, NY). A compensated attenuator at the laser output allowed adjustment of the remaining laser power (not shown, M-925D, Newport, Irvine, CA). The beam then passed to a commercial laser autocorrelator system (not shown, Mini—Microscope Version, APE Gmbh, Berlin) which allowed the laser pulsewidth to be measured before experiments; during experiments, it permitted the beam to pass through unperturbed. The laser beam was expanded to ~10 mm diameter to fill the 10 × 10 mm square optical aperture of the two orthogonally mounted AODs. An achromatic half-wave ($\lambda/2$) plate (AHWP05M-950, Thorlabs, Newton, NJ) was inserted prior to the first AOD to allow the linearly polarized laser output to be rotated to match the preferred direction for maximum diffraction efficiency at the AODs.

The optical path of the scanning system consists of a series of relay telescopes—lens pairs separated by the sum of their focal lengths both within and between telescopes. This serves to prevent optical ray runoff. The telescope between the two AODs allows the deflectors to virtually reside in the same optical plane, forming a common pivot point for the two-dimensional angular scan pattern. The subsequent telescopes "relay" the pivot point to the back focal aperture (BFA) of the objective. Locating the pivot point at the BFA minimizes light loss due to aperturing and assures telecentric imaging—i.e., minimizes lateral shifts of defocused planes. All of the telescopes were 1× magnification, except for that labeled "Scan Angle Magnification," which magnified the angular scan range by 1.4×. This expanded the angular scan range to approximately 70 mrad, which was sufficient to cover a scan area >200 × 200 μm when coupled into the high magnification water dipping objective lens employed (CFI Fluor 60×/1.0 NA, Nikon Instruments, Melville, NY). Lenses employed throughout AO scanner path were all achromatic doublets, and anti-reflection coated for the near infrared region (Thorlabs and Linos Photonics, Milford, MA). To achieve maximal diffraction efficiency, each AOD was rotated about the axis normal to its deflection plane until maximum intensity in the first order diffracted beam was achieved when tuned to the central acoustic frequency of the RF tuning range. This corresponds to the AOD's characteristic Bragg angle for a given optical wavelength (Gottlieb et al. 1983).

The AO scanning path was coupled into an upright microscope (E600FN, Nikon), via adaptation to the microscope's "Dual Port" camera mount. The excitation was reflected by a retrofitted short-pass dichroic mirror (750DCSP, Chroma Technologies, Rockingham, VT) located in this camera port and transmitted through a long-pass dichroic mirror (700DCXR, Chroma) housed within a filter cube mounted into the microscope's filter slider. When this filter was slid out of the path, fluorescence emission could be visualized using a camera (as in Fig. 2*A*). Normally, fluorescence was reflected back into a custom *Epi*-detection assembly attached at the microscope's *epi*-illumination port. The detection optical path consisted of an f140 (focal length = 140 mm) lens native to the microscope, and a lens doublet effectively forming an f25 lens. The f140 and f25 lenses were located focal distances away from the objective's back focal aperture (BFA) and Photomultiplier tube (PMT) cathode, respectively, and provided afocal demagnification of the BFA onto the photocathode by 5.6× (= 140/25). The detection path consisted also of one or more emission filters. At all times, at least one emission filter was inserted that was specified for high rejection (attenuated to <10^{-5}) throughout the Ti:S tuning range—either an HQ600/200M or HQ500/100M (both Chroma).

Laser pulsewidth and optimization

To mitigate effects of both spatial and temporal dispersion (Iyer et al. 2003), broadened laser pulsewidths of $\Delta\tau = 500–700$ fs (autocorrelated, FWHM) were employed. To achieve this, two adjustments within the Ti:S laser cavity were implemented. First, the path length through the Brewster prisms (BPs) used for intracavity group velocity dispersion (GVD) compensation was minimized by translating the prisms to maximize the pulsewidth to the greatest extent possible before spectral components were truncated by the prism tips. The spectrum and laser pulsewidth were found to inversely vary, as expected for intracavity GVD adjustments. This procedure led to a maximum pulsewidth of $\Delta\tau \sim 300$ fs (autocorrelated) without any loss of output power. Second, the cavity's inner end mirror could be adjusted to restrict the spectral content within the laser pulse. This allowed the pulsewidth to be further broadened at the expense of reducing the cavity's output power, in a continuous manner. Approximately 60 and 40% of the full cavity power (1 W) was available at $\Delta\tau = 500$ fs and $\Delta\tau = 700$ fs, respectively.

Electronics and software

For RF generation, the two DDS boards generation were interfaced to a digital input/output (DIO) board (PCI-6534, National Instru-
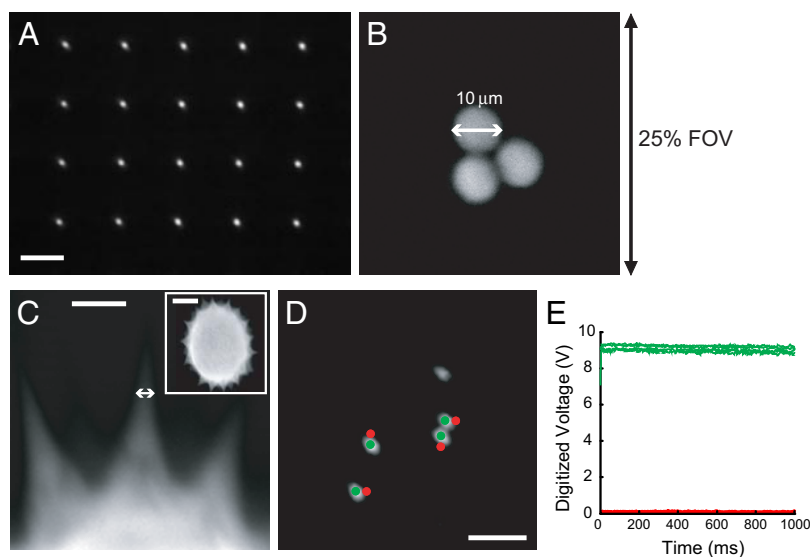
FIG. 2. Validation of RAMP microscope using fluorescent test specimens. *A*: emission from a plastic fluorescent test slide (Chroma) for a continuously scanned sparse square array scan pattern. Image captured by alternate camera path shown in Fig. 1*B*. Scale bar, 10 μm. *B*: image of 10 μm-diam fluorescent beads (F-8836, Molecular Probes) collected using a raster scan spanning 25% of the angular scan range in each dimension. Measured size of bead within image allowed field-of-view size to be estimated as 212 $\times$ 212 μm. *C*: image of stained pollen grain (30-4264, Carolina Biological Supply) taken using a raster scan over a small scan area (13$\times$ zoom). Spine structures are seen to taper to dimensions <1 μm (reference line with arrowheads). Scale bar, 3 μm. *Inset*: image of the entire pollen grain taken at lower zoom factor. Scale bar, 10 μm. *D*: image of 1 μm fluorescent beads (F-13081, Molecular Probes), with user-selected sites directly on (green), and just beside (red, 1 μm separation), several beads for a subsequent random-access scan. Scale bar, 5 μm. *E*: functional image composed of recordings at each site selected in (*D*) was obtained at a frame rate of 1 kHz. Fluorescence was demultiplexed into separate recordings at each site, reported as the digitized voltage from PMT detector and circuit. Sites located on beads produced strong signals of constant intensity (green lines), near the 10-V full scale of the digitizer. Sites beside beads yielded little measurable signal (red lines).

ments, Austin, TX) using custom level shifter electronics. The generated RF waves were subsequently amplified to a full scale value of 2 W (RMS) using the wideband amplifiers contained within a pair of VCO deflector drivers (DE-702M, IntraAction). For detection, a commercial PMT module was employed (H7712-13, Hamamatsu, Hamamatsu City, Japan) based on a R6357 PMT (Hamamatsu). The PMT module contains a built-in regulated high-voltage supply (HVS) and a built-in I/V converter which outputs a 0- to 1-V voltage output. A custom "PMT interface circuit" was employed (shown in Fig. 1*B*) that provided regulated $\pm$12-V power as an input to the HVS, allowed manual adjustment of a 0- to 1.2-V control signal provided to the module determining the PMT gain, provided saturation protection, and interfaced the PMT output to a 5 MHz, 12-bit A/D converter (ADC, PCI-6111, National Instruments).

The RAMP microscope system was controlled using custom software written for the Windows operating system using the .NET framework (Microsoft, Redmond, WA). The software allows for graphical selection of scan areas and sites for raster and random-access scans, respectively (Fig. 1, *C* and *D*). In both cases, linear arrays of RF frequencies were generated for each deflector and translated into digital command sequences to control the DDS boards and a clock signal which triggered ADC samples at the maximum rate at each new site after the access time τ_{access} elapsed. The software also provided support for automated collection of image stacks, using serial port control of a stepper motor (Remote Focus Accessory, Nikon). For recording mode, the DIO pattern could be externally triggered, enabling the optical recording to be synchronized to the current injection specified in separate electrophysiology software (WinWCP, Dr. John Dempster, University of Strathclyde). This software interfaced to the patch-clamp amplifier (BVC-700A, Dagan) via a separate multi-function data-acquisition board (PCI-6040E, National Instruments).

Hippocampal brain slice preparation

Rat hippocampal slices were obtained from the brains of 4- to 6-wk-old Sprague Dawley rats and prepared in accordance with the guidelines of the National Institutes of Health as approved by the animal care and use committee of Baylor College of Medicine. Animals were anesthetized and perfused trans-cardially prior to decerebration and cutting of the slices using a perfusion/cutting solution kept at 2–4°C. This solution consisted of (in mM) 2.5 KCl, 1.25 $Na_2H_2PO_4$, 25 $NaHCO_3$, 0.5 $CaCl_2$, 7 $MgCl_2$, 7 dextrose, 110 choline chloride, 1.3 ascorbate, and 3 pyruvate. Slices (thickness 400 μm)

were cut using a tissue slicer (Vibratome 1000+, Ted Pella, Redding, CA) in this cutting solution. Slices were then transferred to artificial cerebrospinal fluid (containing in mM: 125 NaCl, 2.5 KCl, 1.25 $Na_2H_2PO_4$, 25 $NaHCO_3$, 2 $CaCl_2$, 2 $MgCl_2$, and 10 dextrose) at 35°C for 1 h and then allowed to adjust to room temperature before use.

Experimental procedures

For all experiments, the laser was tuned to 800 nm. The laser pulsewidth was adjusted to 500–700 fs (FWHM) as measured by the autocorrelator. The compensated optical attenuator was used to adjust the laser power to 40–80 mW at the back focal aperture of the objective lens. The higher end of this range was sometimes used for functional imaging, whereas structural imaging was done exclusively at the lower powers.

Hippocampal brain slices were maintained in artificial cerebrospinal fluid (ACSF) containing (in mM, 125 NaCl, 2.5 KCl, 1.25 $Na_2H_2PO_4$, 25 $NaHCO_3$, 2 $CaCl_2$, 2 $MgCl_2$, and 10 dextrose). Solution was bubbled with 95% O_2-5% CO_2. For mapping experiments (as in Figs. 4 and 5), solution was held at 32–34°C using an in-line temperature controller (TC-324B, Warner Instruments, Hamden, CO) unless otherwise specified. Patch pipettes were filled with an intracellular solution consisting of (in mM) 120 K-Gluconate, 20 KCl, 10 HEPES, 2 $MgCl_2$, 4 Mg_2GTP, and 0.3 NaGTP. In addition, the fluorescent label Alexa 594 (50 μM) and fluorescent indicator Oregon Green bis-(o-aminophenoxy)-*N,N,N',N'*-tetraacetic acid (BAPTA)-1 (OGB-1, 200 μM) were included (Molecular Probes, Eugene, OR). Pipettes were pulled to tips of 2–6 MΩ. Cells were held at a resting potential of −65 mV and had an access resistance of 10–20 MΩ. Using IR-DIC imaging, the CA1 region of the hippocampus was identified and candidate pyramidal neurons were selected for patch-clamp recordings in current-clamp mode.

After a loading period of 15–20 min, raster scans (Fig. 1*C*) consisting of 200 $\times$ 200 evenly spaced spots spanning areas of 53 $\times$ 53 μm (4$\times$ zoom) to 212 $\times$ 212 μm (full field of view) were employed at 1–2 s/frame for live visualization of the neuron. A broadband HQ600/200M emission filter (Chroma) was employed during this structural imaging. The specimen and focus were adjusted to select areas and planes of interest. At selected regions, the image was stored and sites-of-interest along the imaged neuronal structure were user-selected via the software graphical user interface (GUI). A single site of interest was always placed in a representative background region of the image. Optical recordings of $[Ca^{2+}]$ transients were carried out at selected sites in a random-access scan (Fig. 1*D*) of

sampling rate f_s = 0.5–1 kHz and 1 s duration. The scan was synchronized to the electrophysiology software/hardware, which allowed $[Ca^{2+}]$ transients to be evoked in the dendrites by back-propagating action potentials (bAPs) generated by three somatic current injections of ~1 nA and 3 ms duration at 20 Hz. Presented data consist of averages of n ~5 (range: 1–11) responses to such stimuli. During optical recordings, the broadband emission filter was replaced by a pair of narrower band-pass filters—HQ550/100M and 535/40M (both Chroma)—to isolate emission from the Ca^{2+} indicator OGB-1. After collection of functional images, structural image stacks were obtained to create maximum projection images and montages. Individual images were collected at 2 s/frame, at axial planes spaced by 1–2 μm traversed using a stepper motor.

Data analysis

Multi-site recording data were analyzed using a custom GUI developed in MATLAB (Mathworks, Natick, MA). The %ΔF/F values reported were calculated according to

$$\%\frac{\Delta F}{F} = 100 \cdot \frac{F - (F_0 - F_b)}{(F_0 - F_b)} \qquad (3)$$

where F is the raw fluorescence voltage signal at the output of the PMT interface circuits, F_b is the average of the whole trace recorded at a representative background site, and F_0 is the average of the fluorescence at each site during the period prior to electrical stimulation. Presented traces were low-pass filtered to 50–100 Hz, using a 300-point zero group-delay FIR filter, to remove residual shot noise. This final signal bandwidth is comparable to those reported in other studies using MPLSM (Goldberg et al. 2004; Waters et al. 2003). To calculate spatial trends, fluorescence transients at each site were quantified by integrating the transient curves during the period of 200–400 ms—termed $(\Delta F/F)_{int}$–after the start of recording, which comprised the period during and 50 ms after the train of three bAPs. The SNR of transients was calculated using the unfiltered data and defined as the peak value divided by the SD of the prestimulus baseline.

RESULTS

Structural and functional imaging using RAMP microscopy

The RAMP microscope developed allows the multiphoton excitation volume of a focused ultrafast laser beam to visit a predefined set of locations—a "scan pattern"—within the specimen plane of the microscope. For example, Fig. 2A shows a camera image of emission from a fluorescent test slide for a sparse square array pattern scanned at a high rate. Unlike with galvanometer-based scanning, no time must be spent traveling between sites; the only delay is a fixed latency per site given by the access time τ_{access} of the acousto-optic deflectors, which is 15 μs in the present system (see METHODS).

The system was designed for operation in two modes—raster scanning and random-access scanning (Fig. 1, C and D)—which are intended to support structural imaging and functional imaging, respectively. In the former mode, a high-density square array (typically 200 × 200) scan pattern is used to collect full-frame images at modest frame rates, revealing the specimen structure. Given the access time of τ_{access} = 15 μs and assuming a practical dwell time of ≥5 μs/pixel for signal integration, frame periods as short as 0.8 s (=$200^2 \cdot 20$ μs) can be obtained. Such frame times are comparable to those obtained by conventional MPLSM systems. The latter mode of random-access scanning, however, is unique to the present

system. Sites of interest located arbitrarily throughout structural images obtained first via raster scans can be user-selected in the software. The focused laser beam is then cycled between these sites; the entire cycle—a functional image "frame"–can occur at high rates for the normal case where the number of sites-of-interest is much less than the number of pixels in the raster scan. Effectively, pixel count can be flexibly traded for increased frame rate. It should be noted that the raster scan mode, as implemented, is a special case of a random-access scan.

We tested the system's functioning in these two modes using fluorescent test preparations. First, structural images of 10 μm fluorescent beads were obtained to measure the field of view spanned by the full frequency tuning range of the AODs. Employing the beads as a calibration reference, the full field of view was estimated as 212 × 212 μm (Fig. 2B). This is consistent with one of the system design criteria to cover most of the field of view of a high-magnification (×60) objective lens to span substantial portions of typical dendrites within individual scans. Next, we imaged stained pollen grains containing fine spine structures which taper to sizes below the diffraction limit. Imaging done over a small subarea, whose size was known based on the field-of-view calibration (Fig. 2C), allowed the system lateral resolution to be determined as ~1 μm. The RAMP microscope thus approached diffraction-limited performance. This can be attributed to the use of laser pulse widths of 500–700 fs with correspondingly narrowed pulse spectra (see METHODS), which served to mitigate, but not eliminate, the deleterious effect of spatial dispersion that AODs are known to impart on ultrafast laser pulses used for multiphoton excitation (Iyer et al. 2003; Lechleiter et al. 2002; Roorda et al. 2004). Such pulses, moreover, are negligibly broadened temporally. Finally, a preparation of 1-μm fluorescent beads was used to verify the functional imaging capability of the system. After collecting a structural image, sites were selected both on and just beside the beads with a site separation of 1 μm. The fluorescence emission was demultiplexed into signals corresponding to each site, showing the presence and absence of fluorescence at sites on and beside the beads, respectively (Fig. 2, D and E).

Structural and functional imaging of hippocampal neurons

We next tested the system for structural and functional imaging of CA1 pyramidal neurons within hippocampal brain slices. Neurons were loaded with the fluorescent label Alexa 594 (50 μM) using a dye-filled micropipette. Structural images using a raster pattern across the full field of view were collected in series of optical sections separated by 1–2 μm, using a stepper motor for axial focusing. Maximum projection images were computed from these image stacks; combining images from a small number (3) of overlapping areas allowed the collection of composite structural images such as that shown in Fig. 3A. The SNR of this image, estimated as the peak image value divided by the average level in background regions, was >10, allowing the complete dendritic morphology consisting of many thin apical oblique and basal branches to be reliably observed. Examination of individual image stacks serves to verify that the optical sectioning capability of multiphoton microscopy was retained by the RAMP microscope
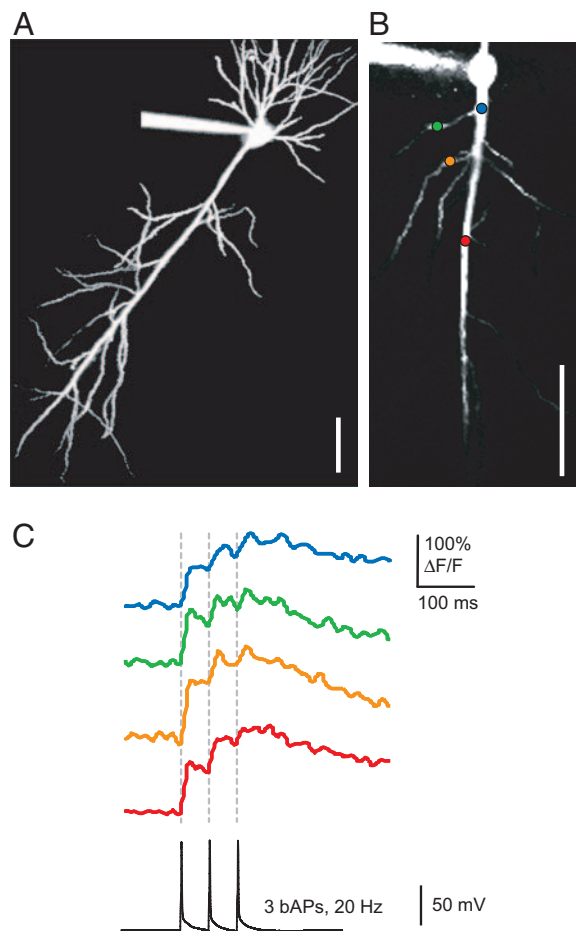
FIG. 3. Structural and functional imaging of neurons in hippocampal brain stices using RAMP microscope. *A*: CA1 pyramidal neuron, loaded with Alexa 594 fluorescent label (50 μM, Molecular Probes). Structural image represents a montage of 3 separate maximum projection images obtained from laterally offset image stacks of raster scans. Axial step size was 2 μm and stacks ranged from 100 to 140 μm in depth. Scale bar, 50 μm. *B*: individual optical section of a CA1 pyramidal neuron co-loaded with Alexa 594 and Ca^{2+}-indicator Oregon Green bis-(o-aminophenoxy)-N,N,N′,N′-tetraacetic acid (BAPTA)-1 (200 μM, Molecular Probes), with sites selected for functional imaging. Scale bar, 50 μm. *C*: functional recordings obtained at sampling rate of 500 Hz from individual sites selected in (*B*) during a stimulation protocol consisting of 3 action potentials (20 Hz) initiated by brief somatic current injections at the soma which back-propagated into the dendrites. Displayed traces are average of *n* = 6 recordings.

(supplemental movie 1). Image collection times for individual optical sections were 1–2 s, similar to that in conventional MPLSM systems.

The primary motivation for developing the RAMP microscope was to allow fast multi-site functional imaging in individual neurons. To test this capability, neurons were co-loaded with Alexa 594 and the Ca^{2+}-sensitive indicator Oregon Green BAPTA-1 (200 μM). Within individual optical sections, sites of interest for functional imaging were selected from throughout a dendritic structure (Fig. 3*B*), which was visualized first via emission from the Alexa 594 indicator as above. Trains of three action potentials (20 Hz) were elicited by current injection into the soma, which propagated actively into the dendrites (Jaffe et al. 1992). These bAPs induced Ca^{2+} transients that

---

[1] The Supplementary Material for this article (a movie) is available online at http://jn.physiology.org/cgi/content/full/00865.2005/DC1.

were concurrently recorded at each of the selected sites (Fig. 3*C*). The high-speed multi-site recording (frame rate of 500 Hz) allowed the synchrony of the sharp onset of transients at all sites to be easily observed, reflecting a rapid spread of bAPs throughout the arbor. This fast functional imaging capability could be extended to greater numbers of sites. A typical example is shown in Fig. 4*A*. The SNR of the averaged (*n* = 6) transients ranged from 5 to 24 (see METHODS). Similar quality recordings have been obtained at >30 sites simultaneously. In general, it was possible to record simultaneously from most or all branches intersecting a given optical section.

When structural images were obtained from subregions of the full field of view (Fig. 4*B*), individual dendritic spines could be visualized (Fig. 4, *C* and *D*). They were found to be ubiquitously present throughout oblique dendritic branches as expected. It was possible to obtain simultaneous recordings of bAP-evoked Ca^{2+} transients from multiple spine heads located throughout these branches (Fig. 4, *C* and *D*). However, we generally regarded imaging and recordings of dendritic spines as at or somewhat beyond the resolution of the present RAMP microscope; the SNR of recordings at the largest spines was noticeably better, reflecting the effect of reduced excitation density caused by the residual spatial dispersion. These recordings nonetheless represent the first demonstration of multi-site recording of fast Ca^{2+} transients in dendritic spines. It is expected that this will be an important application for future versions of the RAMP microscope supporting true diffraction-limited imaging (see DISCUSSION).

Rapid mapping of Ca^{2+} transients in dendrites

The initial results suggested that the present instrument is well suited for structural and functional imaging throughout the entire dendritic structures of central neurons, including the many thin (~1 μm diam) branches that they typically contain. These structures are inaccessible to micropipette approaches and are only partially accessible to wide-field microscopy approaches due to the limited optical sectioning. To apply this capability of the RAMP microscope, we next sought to measure rapidly the spatial pattern of Ca^{2+} transients evoked in the dendrites of CA1 pyramidal neurons, systematically mapping both along their apical trunk and several of their oblique branches, during brief bursts of bAPs. While AP back-propagation into the apical trunk has been extensively mapped, the efficacy of bAP entry into oblique branches has been less well studied due to their inaccessibility via dendritic patch recording. Large numbers of synapses are located on obliques (Megias et al. 2001), and thus the bAP propagation in these branches is of considerable interest, particularly in relation to phenomena such as spike-timing dependent plasticity (Dan and Poo 2004).

For one neuron (Fig. 5*A*), we collected a succession of seven multi-site recordings from different optical sections. In each, several points along the apical trunk and identified oblique branches were selected. In this manner, a comprehensive map of bAP-elicited Ca^{2+} transients was rapidly obtained (Fig. 5*A*). The integrated value of these transients during the bAP train–$(\%\Delta F/F)_{int}$–was employed to quantify the signal at each site (see METHODS). From the values obtained from this cell as well as from three others, spatial trends with respect to location within two defined dendritic compartments, the apical trunk
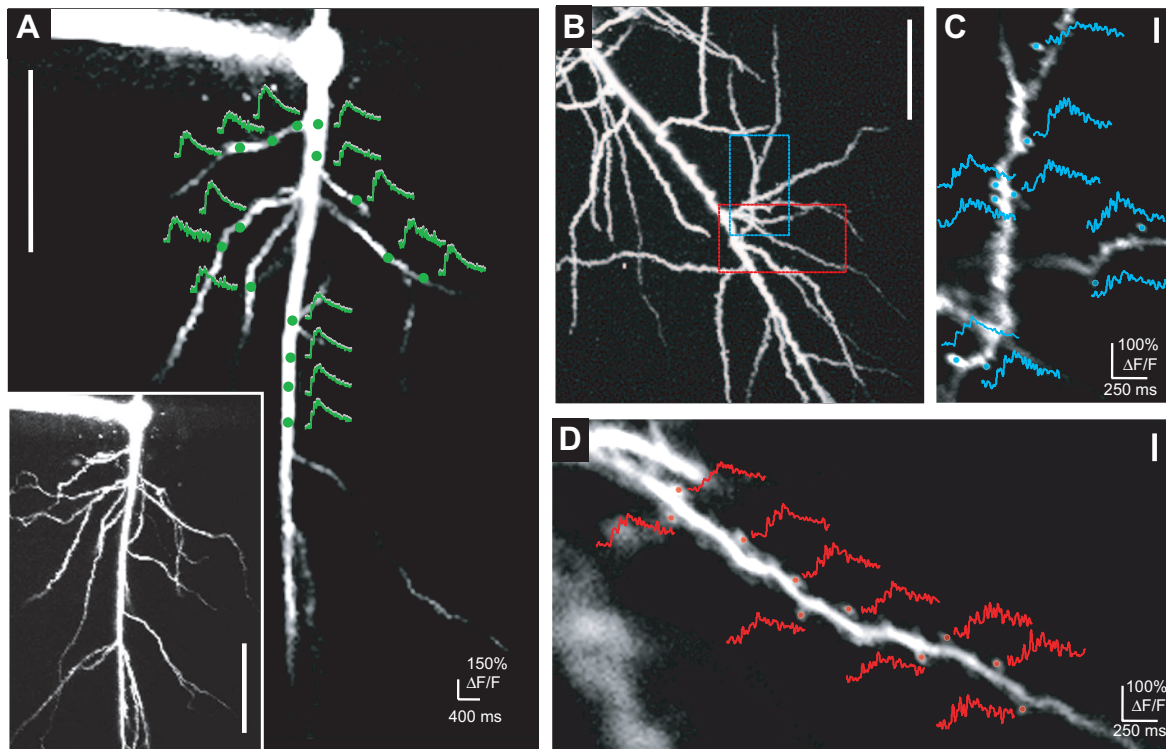
FIG. 4.   Functional imaging of Ca^{2+} transients throughout dendrites and dendritic spines. *A*: several sites from a single optical section of a CA1 pyramidal were selected which spanned various dendritic compartments, including several thin oblique branches. Optical recordings of Ca^{2+} transients elicited by a burst of 3 back-propagating action potentials (bAPs) were obtained simultaneously at a rate of 500 Hz. The multiple recordings shown comprise a "functional image." Displayed traces are obtained from average of $n = 6$ multi-site recordings. *Inset*: maximum projection image computed from an image stack through this neuron reveals full complement of oblique branches emanating from the long apical trunk. Scale bars, 50 μm. *B*: maximum projection structural view of several oblique branches of a CA1 pyramidal neuron. Scale bar, 25 μm. Such branches are seen to contain large numbers of spines, which can be clearly identified in images taken from subregions the field of view shown in *C* and *D*, corresponding to *blue* and *red* boxes, respectively. *C* and *D*: Structural images showing individual spines were obtained using dense (200 × 200) raster scan patterns scaled to fit within subregion. Optical recordings of bAP-elicited Ca^{2+} transients were obtained at 1 kHz from sites selected within identified dendritic spines. Averages of $n = 7$ (*C*) and $n = 6$ (*D*) recordings are shown. Scale bars, 1 μm.

and oblique branches, were extracted (Fig. 5, *B* and *C*). Within the apical trunk, the burst-evoked Ca^{2+} transients substantially declined with distance from the soma, sometimes after rising to a peak within the perisomatic region (Fig. 5*B*). These features are similar to those observed by others for Ca^{2+} transients elicited by single bAPs in pyramidal neurons (Frick et al. 2004; Regehr et al. 1992; Waters et al. 2003) and reflect the decline in the bAP amplitude that has been previously reported in these neurons using dendritic patch recordings (Spruston et al. 1995).

From the spatial maps obtained in the four neurons studied here, the Ca^{2+} transients elicited at a total of 81 sites along 14 oblique branches were quantified relative to their respective parent branch point values along the apical trunk (Fig. 5*C*). While the values along the apical trunk ranged considerably (as in Fig. 5*B*), the signals along each oblique branch were consistently similar in magnitude to their parent site values for the first ~60 μm, after which they declined with distance. Interestingly, these results seem to support the findings of a recent study which described such a near-unity ratio in the initial segment as "normalization" of the Ca^{2+} transients along the oblique branches (Frick et al. 2003), particularly in contrast to the increase that might be expected due to the greater surface-to-volume ratio of the thin branches. In some, but not all, cases transients were also seen to increase within the first 20 μm from the branch point, resulting in an increased mean value in this region. This phenomenon was also observed in the same

study (Frick et al. 2003). Our study demonstrates the viability of using RAMP microscopy to investigate relationships between dendritic structure and function at high spatial resolution—with greatly reduced time and effort.

Rapid mapping of pharmacological effects in dendrites

The functional mapping capability of RAMP microscopy can be combined with the application of pharmacological agents to infer the distribution and role of ion channels in various dendritic compartments. As an example, we considered the effect of 4-aminopyridine (4-AP), which blocks fast A-type K^+ channels, on bAP burst-elicited Ca^{2+} transients. Transients measured before and during bath application of 4-AP (4 mM) at selected sites throughout a CA1 pyramidal neuron are shown in Fig. 6*A*. The RAMP microscope allowed the global effect of the drug—the Ca^{2+} transients were increased in amplitude throughout both the apical trunk and the oblique branches—to be clearly identified within this single experiment.

Previous work based on dendritic patch clamp recordings have shown that the A-type currents (I_A) mediated by these K^+ channels increase with distance along the apical trunk of CA1 pyramidal neurons (Hoffman et al. 1997; Yuan et al. 2002), largely causing the decline of bAP amplitude seen there (as in Fig. 5*B*). Their role or presence in oblique branches, however, could not be investigated using patch-clamp recordings. Using
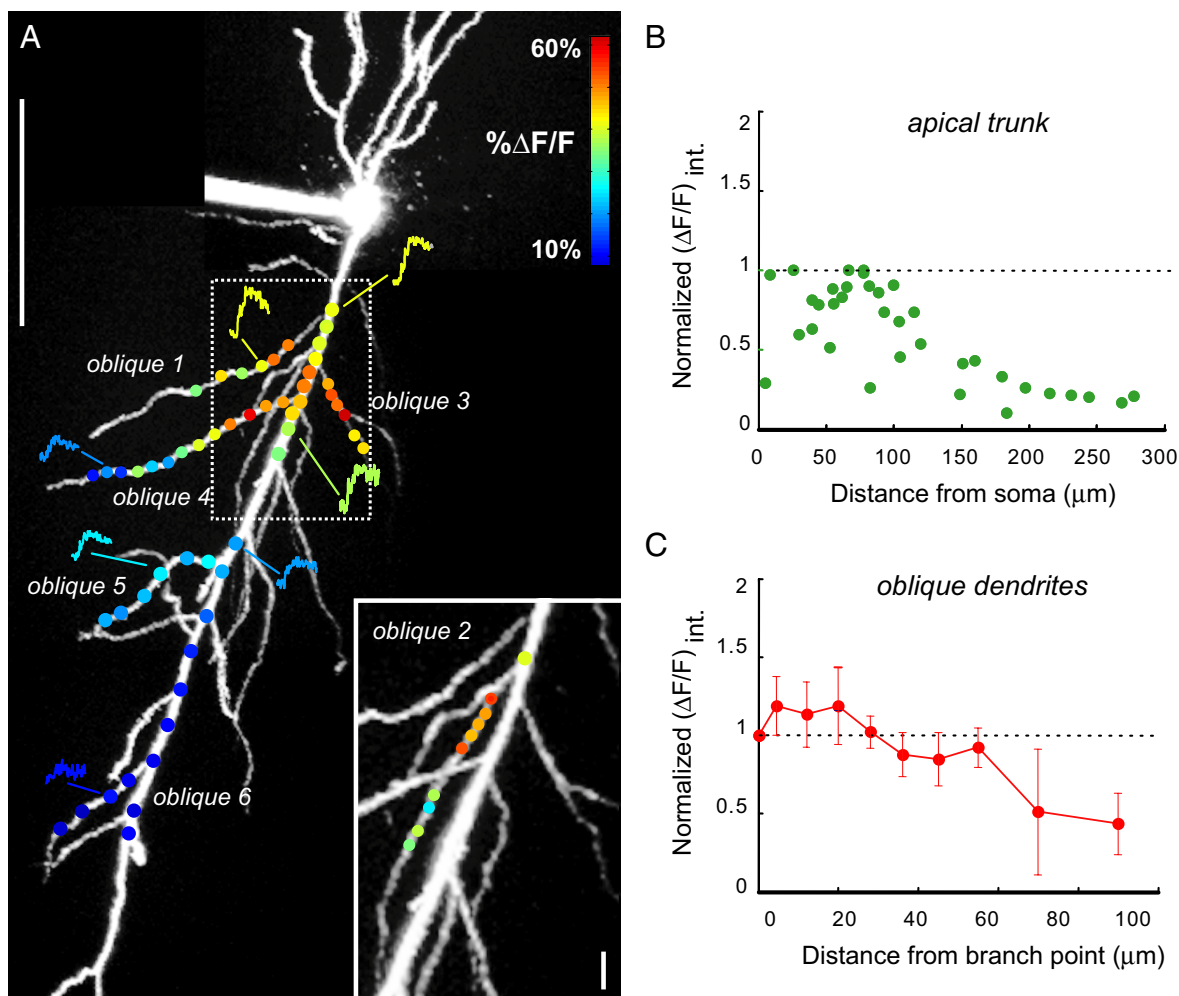
FIG. 5.   Rapid mapping of dendritic Ca^{2+} transients. *A*: maximum projection image montage of a CA1 pyramidal neuron from which a set of seven multi-site recordings were obtained at 500 Hz. Two of the sections were also laterally translated with respect to the others, allowing a larger area of the neuron to be mapped. Recording sites were selected to trace along 6 apical oblique dendrites, 1 shown in *inset*, and the apical trunk. Ca^{2+} transients were obtained at all sites in response to 3 elicited bAPs at 20 Hz. Values of %$\Delta F/F$ were integrated (i.e., averaged) over a time window of 200 ms after onset of stimulus and normalized globally across all sites. Sites are color-coded by the obtained mean transient values according to the provided color map. Representative Ca^{2+} transients are shown at several sites. Scale bar, 50 μm (5 μm in *inset*). *B*: Ca^{2+} transients obtained at various sites along the apical trunks of 3 different neurons including those from *A*. Values of integrated %$\Delta F/F$, shown as (%$\Delta F/F)_{int}$, were normalized to the peak value obtained for each neuron. Signals were seen to decline with distance from the soma. *C*: Ca^{2+} transients recorded in 14 oblique branches at a total of $n = 81$ sites were pooled from 4 neurons, including those from *A*. Measurements along branches were binned into groups according to their distance from their branch point on apical trunk. (%$\Delta F/F)_{int}$ values were normalized relative to the measurements at these parent sites. Normalized transients were seen to be near unity along 1st 60 μm of oblique branches before declining with distance. Variability within each group expressed as means $\pm$ SE.

the RAMP microscope, recordings were obtained both before and during application of 4-AP (4 mM) from multiple sites located throughout three different neurons, including those depicted in Fig. 6*A*, targeting in particular sites located along identified oblique branches. The Ca^{2+} transients, quantified by their integrated values (%$\Delta F/F)_{int}$, were increased at all sites in the presence of 4-AP, both within the apical trunk (drug/control: 1.4–4.6, mean 2.6, $n = 16$) and along the length of oblique branches (drug/control: 1.2–4.2, mean 2.3, $n = 35$).

The consistent observation of an effect at sites along oblique branches does not of itself suggest the presence of A-type K^+ channels within those branches because increased bAP amplitudes in the apical trunk could alone explain the effect. To discriminate between these alternatives, the drug effect was quantified in the oblique branches as a function of distance from their parent branch points, revealing an increasing trend ([*]$P < 0.05$, Fig. 6*B*). Such a trend cannot be explained by an

effect in the apical trunk alone, and suggests that A-type K^+ channels are both present and functionally active within the oblique branches of CA1 neurons. This is consistent with the conclusions of recent studies (Frick et al. 2003, 2004).

DISCUSSION

The present study demonstrates the viability of RAMP microscopy, marking the first time that it has been possible to optically record fast physiological transients at high lateral and axial resolution concurrently from multiple sites located throughout the dendrites of a single neuron within acute brain slices. By allowing recordings from >10 sites simultaneously, the RAMP microscope system represents at least an order-of-magnitude advance over existing multiphoton or confocal laser scanning systems, while also avoiding the substantial sacrifice of resolution and depth penetration that wide-field microscopy
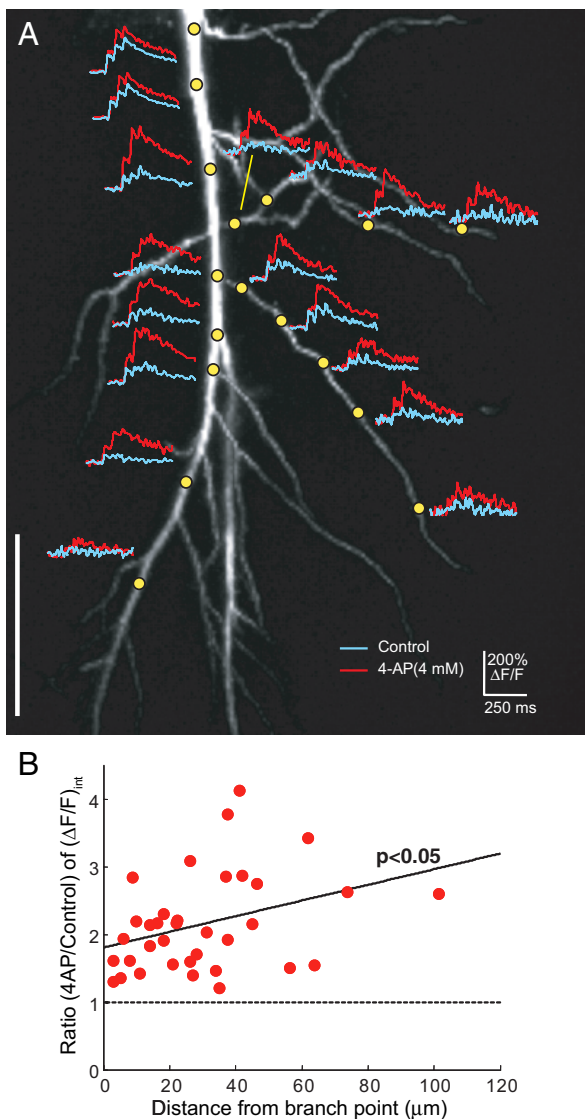
FIG. 6. Rapid mapping of pharmacological effects in dendrites. *A*: maximum projection image obtained from a stack of images, revealing the apical dendrites of a CA1 pyramidal neuron. Scale bar, 50 μm. Recording sites selected from a single optical section are superimposed. Ca^{2+} transients were recorded from these sites at 500 Hz. Transients were elicited by 3 20-Hz bAPs at 34°C either before ($n = 6$, blue traces) or during ($n = 4$, red traces) application of 4-aminopyridine (4-AP, 4 mM). *B*: drug effect (ratio of integrated %$\Delta F/F$, drug/control) from sites along 7 different oblique branches (3 different cells) showing an increasing trend with distance from their parent branch points on apical trunk ($n = 36$, $^*P < 0.05$).

number of sites and their individual sampling rate (the overall frame rate) in a flexible manner, e.g., 50 sites can be visited at 1 kHz, 100 at 500 Hz, etc. Because the branching structure of neurons inherently leads to sparse images, most or all of the sites intersecting a given optical section can be recorded from at high sampling rates.

In the present study, this flexible capability was employed to measure fast Ca^{2+} transients throughout dendrites at >10 sites. Functional mapping of Ca^{2+} signaling elicited by APs or synaptic activation has been the subject of much recent research. This has included investigations regarding the extent to which such signaling is global or local in varying neuronal classes (Goldberg et al. 2005), the existence and locations of excitation "hot spots" (Kaiser et al. 2001), the location and spread of Ca^{2+} waves (Larkum et al. 2003), and the presence of localized alterations in excitability (Frick et al. 2004). These studies have employed optical approaches rather than micropipette techniques, reflecting both the fundamental requirement to access thin dendritic compartments and the practical need for streamlined collection of mapping data. The capabilities of RAMP microscopy demonstrated here are well suited to accelerate significantly this wide range of active research directions, allowing consideration under more experimental conditions and in a larger variety of neuronal classes. Additionally, the ability to collect high-resolution optically sectioned images affords the possibility of carrying out studies tightly coupled to compartmental modeling of neurons. This can further investigations linking the role of dendritic branch morphology to neuronal function (Aizenman et al. 2003; Schaefer et al. 2003; Vetter et al. 2001).

The maximum aggregate sampling rate of RAMP microscopy also fundamentally supports two further advances. First, the system should support Ca^{2+} transient (frame rates ≤ 500 Hz) recordings from ~ 100 sites—representing a two order-of-magnitude increase in measurement throughput. For many neurons, such as the pyramidal cells employed here, the many structures of which generally cross the specimen plane, this practically requires an added capability for fast three-dimensional focusing, which is being pursued further in this laboratory (see following text). Some neurons, however, have relatively planar dendrites and should be well suited to very high-throughput recordings using the present two-dimensional instrument. A particular example is Purkinje cells, for which studies to date have already revealed a range of spatially compartmentalized patterns of activation (Callaway et al. 1995; Wang et al. 2000). Second, the system also supports the use of high sampling rates >1 kHz at ≤ 10 s of sites, fundamentally allowing direct measurement of membrane potential transients. We have previously demonstrated the use of random-access microscopy to acquire multi-site recordings of membrane potential transients in low-density neuronal cultures using voltage-sensitive dyes (Bullen and Saggau 1997, 1999). The optical sectioning capability of RAMP microscopy promises to allow such measurements to be obtained from more physiologically relevant specimens—acute brain slices. Recent work describing improvements in voltage sensitivity of indicators using nonlinear excitation (Dombeck et al. 2005; Kuhn et al. 2004) offers encouragement that rapidly mapping membrane potential transients using RAMP microscopy may soon be practically possible.

approaches entail. The system thus combines high-throughput functional mapping with high-resolution structural imaging capability, providing a single tool well suited to investigating the various degrees and forms of compartmentalized signaling and processing arising within individual neurons of the CNS.

The distinguishing technical feature of RAMP microscopy is its ability to provide high-resolution site-directed multiphoton excitation to any lateral position within the microscope's field of view. This performance can be stated in terms of an aggregate sampling rate, which in the present system is maximally ~ 50 kHz, calculated from the repositioning time of 15 μs and a practical minimal dwell time for recording of 5 μs. This aggregate sampling rate can be allocated between the

The present system should be compared with other approaches that have been described to achieve fast imaging using multiphoton excitation, such as the use of a resonant galvanometer (Fan et al. 1999; Tan et al. 1999) or multifocal multiphoton microscopy (Straub et al. 2000). Acousto-optic deflection and multiphoton microscopy have also been previously combined to similarly allow fast imaging (Lechleiter et al. 2002; Roorda et al. 2004), using a single AOD combined with a galvanometer-driven scanning mirror. This configuration provides some advantage over the use of a resonant galvanometer, offering a true linear scan. However, by scanning only rectangular regions, none of these approaches allow the beam dwell time to be allocated exclusively where it is required, making it difficult to achieve high signal-to-noise ratio recordings at high sampling rates from small dendritic compartments with existing indicators. Consequently, they have been limited to video-rate recordings of relatively larger and slower signals. Only the use of random-access scanning enabled by two-dimensional acousto-optic deflection attains the stringent spatial and temporal requirements posed by dendritic functional imaging.

As mentioned in the preceding text, a two-dimensional acousto-optic laser scanning system has been previously developed in this laboratory for single-neuron studies (Bullen and Saggau, 1999). That system, however, employed a visible laser for single-photon excitation, which provided no intrinsic optical sectioning. It was thus suited only for the study of dissociated hippocampal cultures—effectively two-dimensional preparations—to avoid light scattering problems. In contrast, the use of multiphoton excitation in the present instrument allows measurements to be obtained from within the volume of physiologically realistic brain tissue slice preparations. Furthermore, the lateral resolution was improved at least twofold relative to the original instrument, owing to the use of a large-area AO deflector. We believe the RAMP microscope thus represents a significant improvement relative to the range of nonsectioning systems used to date for multi-site optical recording, including both previous acousto-optic scanners and the wide-field imaging techniques which have been discussed.

In the present system, broadened laser pulse widths of 500–700 fs were employed. This served to mitigate, but not eliminate, much of the spatial dispersion associated with acousto-optic deflection of the ultrafast pulses used for multiphoton excitation. To attain fully diffraction-limited imaging, future versions of the RAMP microscope could employ more conventional pulsewidths of ~100 fs along with auxiliary spatial dispersion compensation components described by us and others (Iyer et al. 2003; Lechleiter et al. 2002; Roorda et al. 2004). This should enable imaging of neurons deeper within brain tissue as well as more robust multi-site recordings from dendritic spines. This latter capability would permit fast collection of statistics on the functional characteristics of spines and the rich variety of modulations thereof (Hoogland et al. 2004; Sabatini and Svoboda 2000 Yasuda et al. 2003). Another limitation of the present instrument is the restriction of fast scanning to within a given optical section. Axial scanning was done by slower mechanical translation of the objective focusing mechanism using a stepper motor. This hinders the ability to record from throughout an identified neuronal compartment, such as a particular oblique branch in pyramidal neurons, within a single scan, given that these generally do not reside in a single focal plane. This limitation may be overcome by a new AOD-based scanning scheme, for which we recently obtained a proof-of-principle in our lab, that allows fast three-dimensional positioning, while also intrinsically compensating for spatial dispersion without auxiliary elements (Reddy and Saggau 2005).

Finally, it should be noted that RAMP microscopy is apt to have broader application to experimental neuroscience beyond recordings in single neurons as presented here. In particular, it should enable the possibility of multi-site uncaging of neurotransmitter to simulate realistic clustered and distributed patterns of synchronous synaptic activation, at the level of single spines (Matsuzaki et al. 2004). In addition, RAMP microscopy should be applicable to larger scan areas, allowing the patterns of cellular activation in neural networks to be recorded at significantly higher rates than presently possible (Brustein et al. 2003; Ikegaya et al. 2004; Ohki et al. 2005). This promises to enhance the detection of synchrony across many disparate cells. Although images of neural networks are not necessarily sparse, the numbers of cells contained therein are, and thus the same advantages of random-access scanning apply.

REFERENCES

Aizenman CD, Huang EJ, and Linden DJ. Morphological correlates of intrinsic electrical excitability in neurons of the deep cerebellar nuclei. *J Neurophysiol* 89: 1738–1747, 2003.

Antic S, Major G, and Zecevic D. Fast optical recordings of membrane potential changes from dendrites of pyramidal neurons. *J Neurophysiol* 82: 1615–1621, 1999.

Brustein E, Marandi N, Kovalchuk Y, Drapeau P, and Konnerth A. "In vivo" monitoring of neuronal network activity in zebrafish by two-photon Ca(2+) imaging. *Pfluegers* 446: 766–773, 2003.

Bullen A, Patel SS, and Saggau P. High-speed, random-access fluorescence microscopy. I. High-resolution optical recording with voltage-sensitive dyes and ion indicators. *Biophys J* 73: 477–491, 1997.

Bullen A and Saggau P. High-speed, random-access fluorescence microscopy. II. Fast quantitative measurements with voltage-sensitive dyes. *Biophys J* 76: 2272–2287, 1999.

Callaway JC, Lasser-Ross N, and Ross WN. IPSPs strongly inhibit climbing fiber-activated $[Ca^{2+}]i$ increases in the dendrites of cerebellar Purkinje neurons. *J Neurosci* 15: 2777–2787, 1995.

Dan Y and Poo MM. Spike timing-dependent plasticity of neural circuits. *Neuron* 44: 23–30, 2004.

Denk W, Strickler JH, and Webb WW. Two-photon laser scanning fluorescence microscopy. *Science* 248: 73–76, 1990.

Djurisic M, Antic S, Chen WR, and Zecevic D. Voltage imaging from dendrites of mitral cells: EPSP attenuation and spike trigger zones. *J Neurosci* 24: 6703–6714, 2004.

Dombeck DA, Sacconi L, Blanchard-Desce M, and Webb WW. Optical recording of fast neuronal membrane potential transients in acute mammalian brain slices by second-harmonic generation microscopy. *J Neurophysiol* 2005.

Fan GY, Fujisaki H, Miyawaki A, Tsay RK, Tsien RY, and Ellisman MH. Video-rate scanning two-photon excitation fluorescence microscopy and ratio imaging with cameleons. *Biophys J* 76: 2412–2420, 1999.

Frick A, Magee J, and Johnston D. LTP is accompanied by an enhanced local excitability of pyramidal neuron dendrites. *Nat Neurosci* 7: 126–135, 2004.

Frick A, Magee J, Koester HJ, Migliore M, and Johnston D. Normalization of Ca^{2+} signals by small oblique dendrites of CA1 pyramidal neurons. *J Neurosci* 23: 3243–3250, 2003.

Goldberg JH, Lacefield CO, and Yuste R. Global dendritic calcium spikes in mouse layer 5 low threshold spiking interneurones: implications for control of pyramidal cell bursting. *J Physiol* 558: 465–478, 2004.

Goldberg JH and Yuste R. Space matters: local and global dendritic Ca(2+) compartmentalization in cortical interneurons. *Trends Neurosci* 28: 158–167, 2005.

Gottlieb M, Ireland CLM, and Ley JM. *Electro-Optic and Acousto-Optic Scanning and Deflection.* New York: Dekker, 1983.

Hausser M and Mel B. Dendrites: bug or feature? *Curr Opin Neurobiol* 13: 372–383, 2003.

Hoffman DA, Magee JC, Colbert CM, and Johnston D. K^+ channel regulation of signal propagation in dendrites of hippocampal pyramidal neurons. *Nature* 387: 869–875, 1997.

Hoogland TM and Saggau P. Facilitation of L-type Ca^{2+} channels in dendritic spines by activation of beta2 adrenergic receptors. *J Neurosci* 24: 8416–8427, 2004.

Ikegaya Y, Aaron G, Cossart R, Aronov D, Lampl I, Ferster D, and Yuste R. Synfire chains and cortical songs: temporal modules of cortical activity. *Science* 304: 559–564, 2004.

Iyer V, Losavio BE, and Saggau P. Compensation of spatial and temporal dispersion for acousto-optic multiphoton laser-scanning microscopy. *J Biomed Opt* 8: 460–471, 2003.

Jaffe DB, Fisher SA, and Brown TH. Confocal laser scanning microscopy reveals voltage-gated calcium signals within hippocampal dendritic spines. *J Neurobiol* 25: 220–233, 1994.

Jaffe DB, Johnston D, Lasser-Ross N, Lisman JE, Miyakawa H, and Ross WN. The spread of Na^+ spikes determines the pattern of dendritic Ca^{2+} entry into hippocampal neurons. *Nature* 357: 244–246, 1992.

Johnston D, Christie BR, Frick A, Gray R, Hoffman DA, Schexnayder LK, Watanabe S, and Yuan LL. Active dendrites, potassium channels and synaptic plasticity. *Philos Trans R Soc Lond B Biol Sci* 358: 667–674, 2003.

Kaiser KM, Zilberter Y, and Sakmann B. Back-propagating action potentials mediate calcium signalling in dendrites of bitufted interneurons in layer 2/3 of rat somatosensory cortex. *J Physiol* 535: 17–31, 2001.

Kuhn B, Fromherz P, and Denk W. High sensitivity of Stark-shift voltage-sensing dyes by one- or two-photon excitation near the red spectral edge. *Biophys J* 87: 631–639, 2004.

Larkum ME, Watanabe S, Nakamura T, Lasser-Ross N, and Ross WN. Synaptically activated Ca^{2+} waves in layer 2/3 and layer 5 rat neocortical pyramidal neurons. *J Physiol* 549: 471–488, 2003.

Larkum ME and Zhu JJ. Signaling of layer 1 and whisker-evoked Ca^{2+} and Na^+ action potentials in distal and terminal dendrites of rat neocortical pyramidal neurons in vitro and in vivo. *J Neurosci* 22: 6991–7005, 2002.

Lechleiter JD, Lin DT, and Sieneart I. Multi-photon laser scanning microscopy using an acoustic optical deflector. *Biophys J* 83: 2292–2299, 2002.

Matsuzaki M, Honkura N, Ellis-Davies GC, and Kasai H. Structural basis of long-term potentiation in single dendritic spines. *Nature* 429: 761–766, 2004.

Megias M, Emri Z, Freund TF, and Gulyas AI. Total number and distribution of inhibitory and excitatory synapses on hippocampal CA1 pyramidal cells. *Neuroscience* 102: 527–540, 2001.

Ohki K, Chung S, Ch'ng YH, Kara P, and Reid RC. Functional imaging with cellular resolution reveals precise micro-architecture in visual cortex. *Nature* 433: 597–603, 2005.

Polsky A, Mel BW, and Schiller J. Computational subunits in thin dendrites of pyramidal cells. *Nat Neurosci* 7: 621–627, 2004.

Reddy GD and Saggau P. Fast three-dimensional scheme scanning using acousto-optic deflectors. *J Biomed Opt* In press.

Regehr WG and Tank DW. Calcium concentration dynamics produced by synaptic activation of CA1 hippocampal pyramidal cells. *J Neurosci* 12: 4202–4223, 1992.

Roorda RD, Hohl TM, Toledo-Crow R, and Miesenbock G. Video-rate nonlinear microscopy of neuronal membrane dynamics with genetically encoded probes. *J Neurophysiol* 92: 609–621, 2004.

Ross WN and Werman R. Mapping calcium transients in the dendrites of Purkinje cells from the guinea-pig cerebellum in vitro. *J Physiol* 389: 319–336, 1987.

Sabatini BL and Svoboda K. Analysis of calcium channels in single spines using optical fluctuation analysis. *Nature* 408: 589–593, 2000.

Schaefer AT, Larkum ME, Sakmann B, and Roth A. Coincidence detection in pyramidal neurons is tuned by their dendritic branching pattern. *J Neurophysiol* 89: 3143–3154, 2003.

Spruston N, Schiller Y, Stuart G, and Sakmann B. Activity-dependent action potential invasion and calcium influx into hippocampal CA1 dendrites. *Science* 268: 297–300, 1995.

Straub M, Lodemann P, Holroyd P, Jahn R, and Hell SW. Live cell imaging by multifocal multiphoton microscopy. *Eur J Cell Biol* 79: 726–734, 2000.

Stuart GJ, Dodt HU, and Sakmann B. Patch-clamp recordings from the soma and dendrites of neurons in brain slices using infrared video microscopy. *Pfluegers* 423: 511–518, 1993.

Svoboda K, Helmchen F, Denk W, and Tank DW. Spread of dendritic excitation in layer 2/3 pyramidal neurons in rat barrel cortex in vivo. *Nat Neurosci* 2: 65–73, 1999.

Tan YP, Llano I, Hopt A, Wurriehausen F, and Neher E. Fast scanning and efficient photodetection in a simple two-photon microscope. *J Neurosci Methods* 92: 123–135, 1999.

Tank DW, Sugimori M, Connor JA, and Llinas RR. Spatially resolved calcium dynamics of mammalian Purkinje cells in cerebellar slice. *Science* 242: 773–777, 1988.

Vetter P, Roth A, and Hausser M. Propagation of action potentials in dendrites depends on dendritic morphology. *J Neurophysiol* 85: 926–937, 2001.

Wang SS, Denk W, and Hausser M. Coincidence detection in single dendritic spines mediated by calcium release. *Nat Neurosci* 3: 1266–1273, 2000.

Waters J, Larkum M, Sakmann B, and Helmchen F. Supralinear Ca^{2+} influx into dendritic tufts of layer 2/3 neocortical pyramidal neurons in vitro and in vivo. *J Neurosci* 23: 8558–8567, 2003.

Yasuda R, Sabatini BL, and Svoboda K. Plasticity of calcium channels in dendritic spines. *Nat Neurosci* 6: 948–955, 2003.

Yuan LL, Adams JP, Swank M, Sweatt JD, and Johnston D. Protein kinase modulation of dendritic K^+ channels in hippocampus involves a mitogen-activated protein kinase pathway. *J Neurosci* 22: 4860–4868, 2002.

Yuste R and Denk W. Dendritic spines as basic functional units of neuronal integration. *Nature* 375: 682–684, 1995.

Zhang W and Linden DJ. The other side of the engram: experience-driven changes in neuronal intrinsic excitability. *Nat Rev Neurosci* 4: 885–900, 2003.